PAPER • OPEN ACCESS

Fiber suspension investigation in a backward-facing step by PIV

View the article online for updates and enhancements.

Fiber suspension investigation in a backward-facing step by PIV

A Capone[1]**, G P Romano**[2]**, A Soldati**[3]

[1]CNR-INSEAN Via di Vallerano 139, Rome Italy
[2]Dipartimento Ingegneria Meccanica e Aeronautica, Università La Sapienza,
Via Eudossiana 18, Rome Italy
[3]Dipartimento Politecnico, Università di Udine, Via delle Scienze 208, Udine Italy

alessandro.capone@cnr.insean.it

Abstract. A dilute suspension (volume fraction 0.05%) of rod-like particles in a turbulent backward-facing step flow at Reynolds number Re_H=14900, is investigated by means of Particle Image Velocimetry. Two-way interactions between fluid and dispersed phase are analyzed by exploiting the high spatial resolution of the acquisitions. Mutual interactions between phases can be investigated by considering flow turbulence modulations and phenomena related to preferential concentration and orientation of fibers. Slight turbulence enhancement is reported in the laden flow and concentration data show a moderate tendency of fibers to accumulate at the channel centreline. Orientation data display a strong preferential orientation of fibers. Local fiber orientation is correlated to the direction of maximum shear showing a high level of correlation also in the flow regions featuring strong gradients.

1. Introduction

In many industrial and environmental applications such as chemical reactors, cyclone separators and devices for pollution abatement, multi-phase turbulent flows in which a carrier fluid is laden with a solid, dispersed phase are commonly encountered.

The understanding of these peculiar suspensions is strongly connected to the investigation of the dynamic interactions between fluid and dispersed phase. An important direction of investigation for engineering applications and of interest for turbulence fundamentals is represented by the study of the impact of the dispersed phase on the flow dynamics, specifically on turbulence modulation. Many efforts have been put forth in this direction ([1], [2] and [3] among others) and a comprehensive review is given in [4]. In addition to the mutual interaction between phases, the distribution and concentration of the dispersed phase is particularly relevant for the study and control of combustion and pollutant dispersion. Several works focused also on this aspect: [5] investigated a forced turbulent jet; homogeneous and isotropic turbulence was investigated by [6]; [7] studied thouroughly preferential concentration of particles induced by turbulence in several configurations. In an unifying perspective, [8] shows how the Stokes number St, defined as the ratio of the particle response time to a

characteristic flow time scale, in combination with the particles volume fraction can describe the interactions in multiphase flows.

Although often the dispersed phase is effectively modeled via spherical particles, there exist many applications where non-isotropic, non-spherical particles are of interest. A particular class of such particles is represented by rod-like particles, characterized by high (>5) aspect ratios.

The dynamics of a single rod-like fiber in shear flow under creeping flow conditions have been theoretically predicted by [9] showing that a fiber tends to align mostly with the mean flow following a periodic revolving motion. Many works have been published on this subject: low-Reynolds number conditions were investigated experimentally by [10] in planar shear flow and by [11] on an inclined plate; contracting channels were investigated by [12]. Turbulent flows at high Reynolds number were studied experimentally by [13], [14] for different contraction shapes, while simulations in channel flow are presented in the works by [15] and [16][17]. To the best of authors' knowledge no experimental work was carried out on rod-like particle laden flows in a turbulent backward-facing step channel.

In this work Particle Image Velocimetry (PIV) is employed to investigate the modification of flow structure and turbulence modulation effects by fibers. Furthermore, fiber concentration and orientation data is extracted and correlated to fluid velocity field so as to shed light on their mutual interactions.

The use of an optical technique as PIV requires a non-trivial image pre-processing step in order to achieve an effective separation of phases. The current experimental set-up makes it possible to employ a discrimination algorithm based on ellipse fitting on fiber images, detailed in [18].
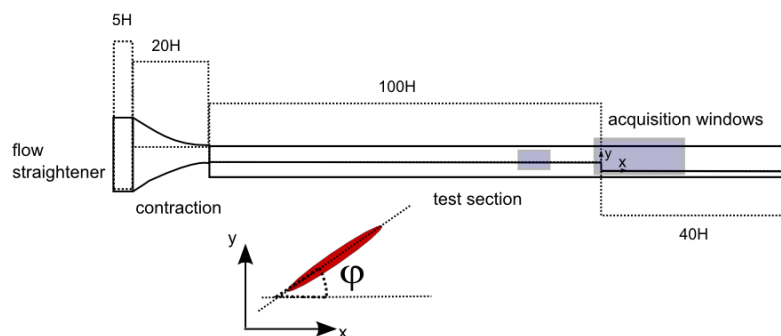

Figure 1 Experimental set-up

2. Experimental set-up

The channel and backward-facing step apparatus is shown in Figure 1. It consists of a channel section approximately 140H long, 2H high and 20H wide, where H=1cm is the step height. The channel section is preceded by a 10:1 contraction in order to reduce turbulence intensity by accelerating the mean flow and by a 5H long flow straightener to increase flow uniformity. The contraction section, which is 20H long, features a polynomial profile to avoid flow separation. At about 100H downstream of the contraction outlet, a backward-facing step is present having an expansion ratio ER=1.5. The flow is driven by a head tank (not shown).

The standard planar, two-component PIV system consists of a 14-bit BW, PCO-Pixelfly CCD camera (1392 X 1040 pixel resolution). The lenses used for all acquisitions are a Nikon F 50 mm with maximum aperture of 1.2. Lighting is provided by a Big Sky Nd:Yag pulsed laser, 488−514 nm, a maximum power equal to 200 mJ. Laser sheet thickness is approximately equal to 1mm. Fluid is seeded with neutrally buoyant 10μm diameter hollow glass spheres (Dantec HGS-10), whereas the dispersed phase is provided by nylon fibers (Polyamide 6.6, density 1.13-1.15g/cm^3, produced by Swissflock AG) with a mean length of approximately L=320μm and a mean diameter of d=24μm so that the aspect ratio k=L/d=13.3. Images were taken in the upstream channel approximately 80H after the 10:1 contraction, thus 20H before the expansion, in a region where the flow can be reasonably

deemed as developed and no disturbance from the step is present, and after the expansion, up to roughly 6H downstream. In order to increase the spatial resolution, this latter acquisition region is subdivided into smaller overlapping parts each covering an area of nearly 1.2H X 1.6H, with a spatial resolution corresponding to 0.012mm/pixel. Acquired image sets consist of 2000 image pairs with an acquisition frequency of 10Hz. A commercial PIV software, DaVis by LaVision Gmbh, has been employed for instantaneous fluid velocity field computation. The minimum window size and overlap were respectively 32x32 and 50%, leading to a vector spacing of 16 pixels corresponding to approximately 0.02H.

Investigation of multiphase flows may be approached with many techniques (a review is given in [19]). In the present case the spatial resolution allows application of the algorithm described in [18], which is based on fiber ellipse fitting.

The experimental campaign was made up of two main acquisitions: a reference case with no fibers in the flow and a fiber-laden cases with volume fraction of C=0.05%. Reynolds number Re_H based on flow centre-line velocity was 14900. The fiber suspension can be considered as dilute because $nL^3 \ll 1$ holds, given n as the number density of fibers.

Single-phase data are validated (not shown) upon comparison to data from [20] collected with a 3D PTV technique in similar experimental conditions.

3. Two-way interaction: fibers to fluid

Based on the classification by [8], multiphase systems may present one-way, two-way and four-way coupling regimes, depending on the extent of the interactions between fluid and dispersed particles and among particles themselves. In the current experiment the volume fraction concentration falls within the 10^{-6}-10^{-3} range where two-way coupling holds. Therefore, the momentum transfer from particles towards the fluid is not negligible and turbulence modulation effects could be observed. Several works ([21], [3] and [1] among others) showed that within this regime, the Stokes number has a particular importance in predicting the quality of modulation.
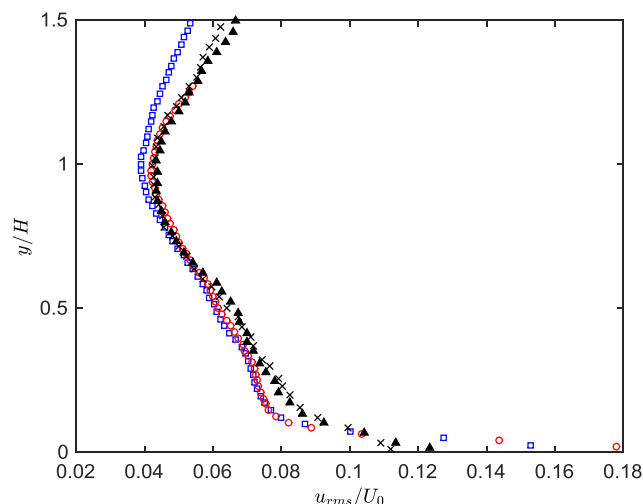

Figure 2 Fluid RMS of streamwise velocity of single phase (blue squares), and fiber-laden (red squares) for the upstream step region. Comparison to data from [22] single-phase (triangles) and multi-phase at 0.00014 volume fraction (crosses).

Figure 3 Fluid RMS of streamwise velocity of single phase (blue squares) and fiber-laden(red squares) in the downstream step region

Figure 4 Fluid turbulent stress mixed term for single phase (blue squares) and fiber-laden (red squares) in the upstream step region. Comparison to data from [22] single-phase (triangles) and multi-phase at 0.00014 volume fraction (crosses).
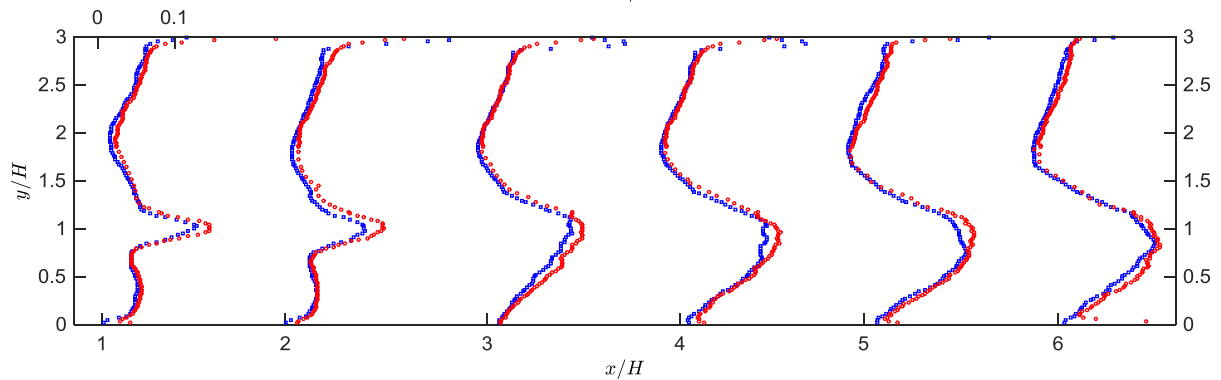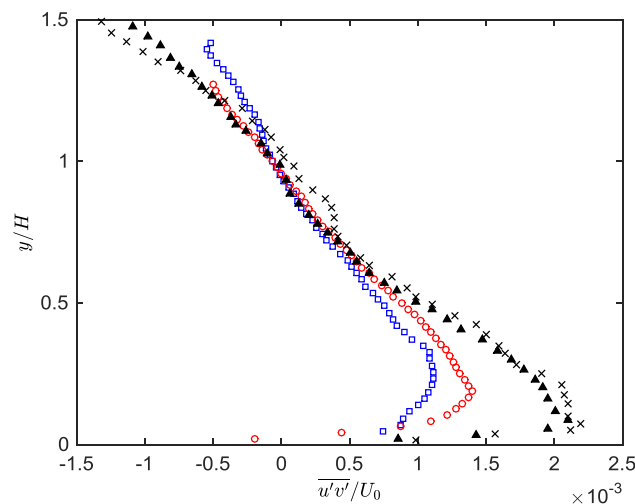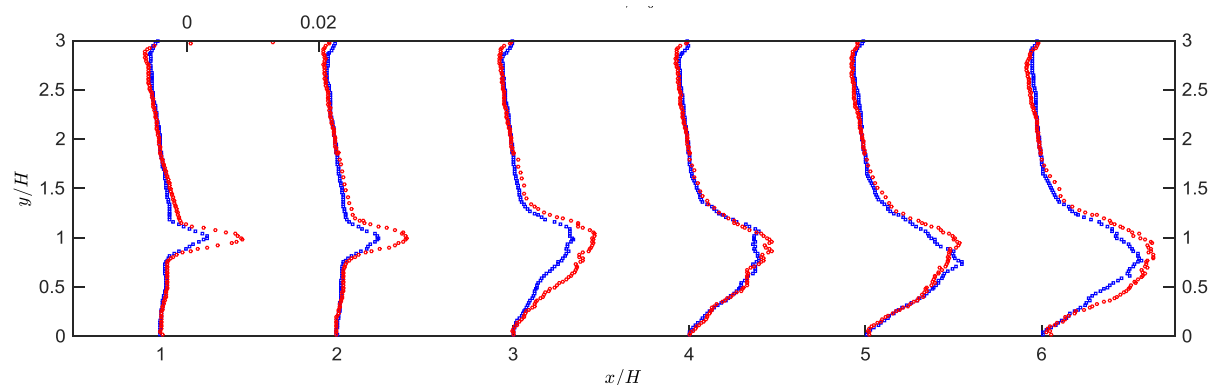

Figure 5 Fluid turbulent stress mixed term for single phase (blue squares) and fiber-laden (red squares) in the downstream step region.

The discussion about the appropriate particle response time, and consequently Stokes number, has been tackled by [17], who pointed out that when the fiber velocity induced by the hydrodynamic drag depends only on fiber characteristic length and D, and if the latter is nearly equal to one, the fiber timescale may be computed, upon choice of fiber length as a characteristic size, as

$$\tau_p = \frac{L}{U_0}$$

In the current conditions, assuming isotropic fiber orientation and adopting as flow timescale τ_f=P/U_0, where P represents the flow integral length scale, it descends that the Stokes number St ranges from 0.2 to 0.5. Specifically, St is larger inside recirculation regions, where on average the flow undergoes steep changes in direction and in these zones strong particle-fluid interactions take place. Outside these regions the Stokes number lies in the lower end and particle inertia effects are weak.

Turbulent intensity profiles are shown in Figure 2 and Figure 3, upstream and downstream the step respectively. Upstream, a slight turbulence enhancement for the laden cases is reported around the channel centre-line as opposed to the data from [22]. Downstream of the step an increase of turbulence in the shear layer up to x/H=2 is observed for the laden conditions. Higher levels are also observed inside the main recirculation bubble, i.e. x/H>2, which is the region where the Stokes number takes on the maximum value. An 1% error introduced by the phase discrimination procedure, should be accounted for.

Reynolds turbulent stress profiles for the upstream and downstream step regions are provided in Figure 4 and Figure 5 and compared to data by [22]. The results in the upstream section, in agreement to the findings of [22] show that the Reynolds stresses (absolute value) are enhanced in the near-wall region and to a larger extent when fibers are present. The extent of this increase is larger downstream of the step and it reaches a 35% increase for x/H=1.

4. Two-way interaction: fluid to fibers

Literature works have shown that conditions characterized by St≈1 correspond to situations where the preferential concentration by turbulence is the strongest ([4], [7]). This considered [7] point out that in water flows, due to the usual small difference between particle and fluid density, preferential concentration does not take place due to the same mechanisms. In fact rod-like particles' dynamics are strongly dependent on orientation and in wall-bounded flows the interactions with boundaries also has an impact on concentration. In the near-wall region, elongated particles are subject to the "pole vaulting" effect described in [10] and [23]. According to the description of this phenomenon, fibers close to the wall are "pole vaulted" away off the wall towards flow regions where they can freely rotate, with this process affecting the equilibrium concentration profile. In Figure 6, the relative local fiber concentration in the channel is compared to results from [24] obtained in a channel at concentration nL^3 =3.6. The concentration distribution in the wall-normal direction is normalized so that the integral of the distribution is equal to the total number of expected fibers divided by nL^3. A marked gradient is reported in the near-wall region, with the relative concentration reaching 90% of the centerline value at approximately 0.2H from the wall. Starting from roughly 0.3H the concentration levels at a nearly constant value. These findings confirm that in the upstream channel the relationships between phases are fully developed and bear resemblance to the findings presented in [25], where fibers were reported to concentrate in core region of a fiber-laden turbulent jet. Insight into fiber orientation dependence on the wall distance is provided by probability density functions (PDF) of fiber orientation computed at different distances from the wall, expressed in terms of the fiber length L. Results are summarised in Figure 7, and confirm that close to the wall, fibers are forced to align along the streamwise direction due to wall physical constraint, whereas as this constraint is relaxed, i.e. for y>L, the PDFs widen.
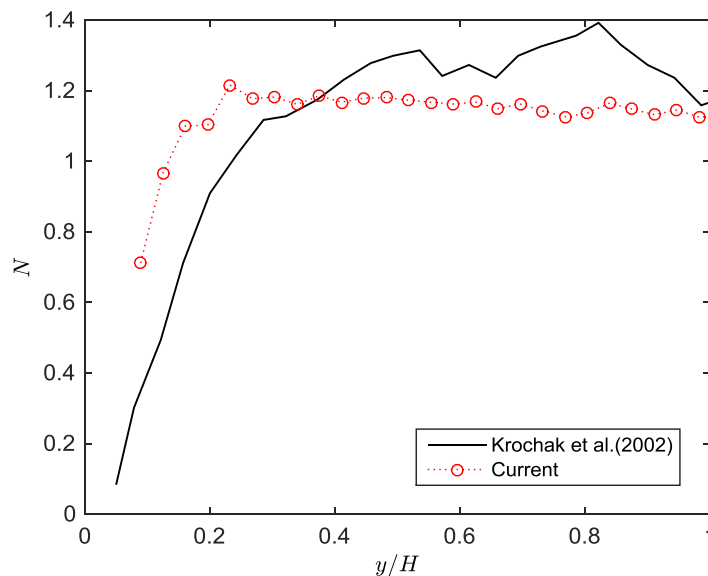
Figure 6 Relative fiber local concentration in the upstream step region.
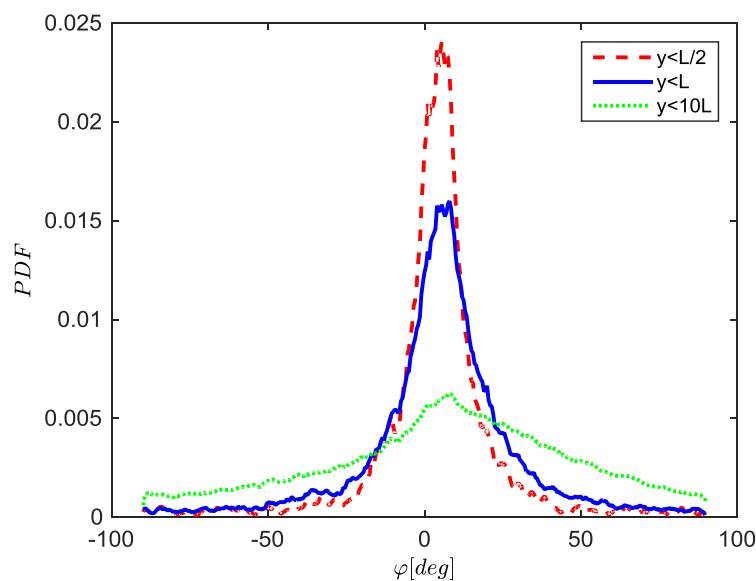

Figure 7 PDF of fiber orientation angle (in degrees as defined in Figure 1 conditioned on wall distance y in the upstream step region.

Several efforts have been carried out to establish a link between fiber mean orientation and some feature of the flow. [10] and [12] [24] focused on low-Reynolds number simple-shear flows, linearly contracting channels and channel contractions with various shapes whereas [26] investigated rods alignment with strain rate in a chaotic flow. Results on global fiber orientation downstream of the step are presented in Figure 8 in terms of mean orientation map and orientation profiles at selected locations.

The map shows the existence of a region featuring slightly negative fiber orientation towards the top of the channel and a region of positive orientations close to the step. This latter region expands towards the bottom when moving downstream, as also the point of sign inversion. Inside the shear layer, fibers take on the largest inclination value, i.e. with an angle roughly equal to 15 degrees, this orientation persisting up to x=5H. Orientation data shown can be effectively associated to turbulence

modulation findings reported in the preceding section. The flow areas where most of the turbulence and turbulent stress modulation effects take place match those where fibers take on the highest orientation angle. A reasonable assumption is that as φ increases, local vortex shedding induced in the surrounding flow is enhanced and turbulence increased. Furthermore, near the bottom side of the step, i.e. for y/H<0.5 x/H<2, a negative orientation region is visible, thus suggesting a relation between orientation and mean flow direction in the lower side of the recirculation bubble.
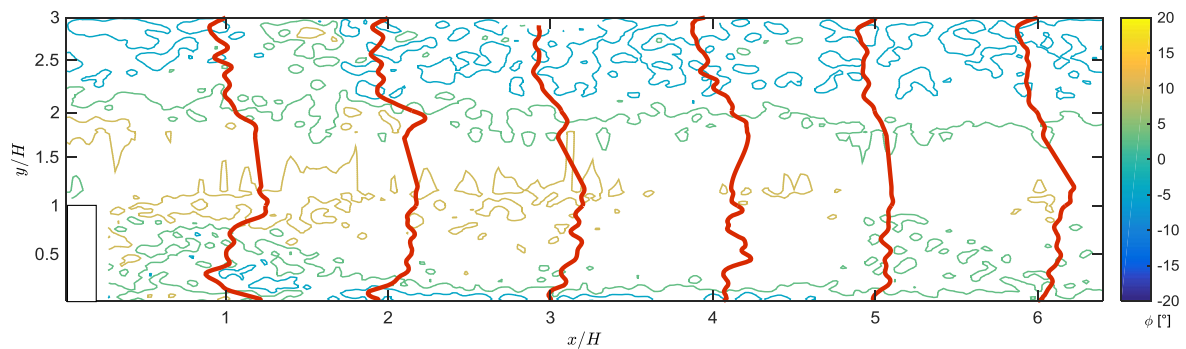

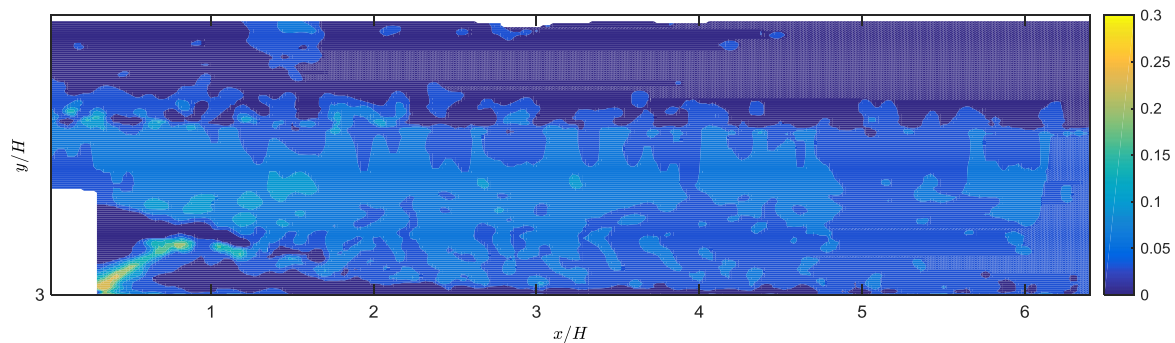**Figure 8** Mean fiber orientation angle map and profiles in downstream step region.

Figure 9 Ratio of angle between fiber and direction of maximum shear to angle of fiber orientation in the downstream step region.

Global alignment of fiber to mean flow direction was assessed based on instantaneous fiber and fluid data. Data were obtained considering instantaneous flow velocity and fibers orientation and obtaining flow velocity at fibers location by tri-linear interpolation of gridded velocity data and averaging the result for each slot, taking into account the resolution/convergence trade-off . Results (not shown) indicate that fibers tend to align to the mean flow with the exception of the flow regions where velocity gradients are stronger. This observation suggests the use of a different parameter rather than local mean flow direction to correlate to fiber orientation. Therefore, fiber orientation has been compared to different directions defined by the flow. In particular, alignment of fibers to strain-rate showed to be weak. Thus, we propose to correlate fibers orientation to the direction of the maximum shear defined as the angle θ for which the following holds

$$\tan 2\theta = -\frac{(\sigma_x - \sigma_y)}{\tau_{xy}}$$

Where σ_x, σ_y and τ_{xy} are respectively the normal stresses along x and y directions and shear stress in the x-y plane. The map of the ratio S = 1-|cosθ|/cosφ is shown Figure 9.

The results show that fibers align to the direction of maximum shear also in the shear layer. Indeed, in the flow region below the main recirculation bubble, S performs very well, with values below 0.05. The stretched thin region between x/H<1 and y/H<0.5 is the one characterized by the poorest

performance of the S index with an average value of 0.17 especially due to developing turbulence. For y/H>1 and on the upper side of the main recirculation bubble fibers alignment to maximum shear plane is still relevant with an average value of S=0.1.

5. Conclusions
The upstream and downstream flow developing in a backward-facing step laden with rod-like particles at dilute concentration is investigated by means of Particle Image Velocimetry. Mean flow structures were reported to be basically unchanged when fibers are present. Moderate turbulence enhancement was reported in the near wall region, in the shear layer and in the recirculation region, as also increments of Reynolds stress cross term in the measurement plane in comparison to unladen conditions. Concentration data show fiber accumulation at the centreline, supposedly due to the combined effect of flow shear and wall physical constraints. Evidence of a marked preferential orientation of fibers is presented. In the channel section, fibers tend to align symmetrically with respect to the centreline. Correlation of fiber orientation angle to the direction of the maximum shear is shown to be strong in general, reaching high levels also in flow region where strong gradients are reported.

References
[1]   Parthasarathy RN and Faeth GM 1990 *J. Fluid Mech.* **220** 485-514
[2]   Rashidi M, Hetsroni G, Banerjee S 1990 *Int. J. Multiph. Flow* **16** 935–949
[3]   Paris AD and Eaton JK 2001 Rep. TSD-137 Dep. Mech. Eng., Stanford Univ.
[4]   Balachandar S, Eaton JK 2010 *Annu Rev. Fluid Mech.* **42** 111-133
[5]   Longmire EK and Eaton JK 1992 *J. Fluid Mech.* **36** 217-257
[6]   Wang LP and Maxey RP 1993 *J. Fluid Mech.* **256** 27-68
[7]   Eaton JK and Fessler JR 1994 *Int. J. Multiphase Flow* **20** 169-209
[8]   Elghobashi L 1994 *App. Sci. Resh.* **52** 309-329
[9]   Jeffery GB 1922 *Fluid Proc. R. Soc. London Ser. A* **102** 161-179
[10]   Moses K, Advani S, Reinhardt A 2001 *Rheol. Acta* **40** 296–396
[11]   Holm R, Soederberg D 2007 *Rheol. Acta* **46** 721–729
[12]   Krochak P, Olson J, Martinez D 2008 *Phys. Fluids* **20** 073303
[13]   Parsheh M, Brown M, Aidun C 2005 *J. Fluid Mech.* **545** 245–269
[14]   Parsheh M, Brown M, Aidun C 2006 *Int. J. Multiph. Flow* **32** 1354–1369
[15]   Marchioli C, Fantoni M, Soldati 2010 A *Phys. Fluids* **22** 033301
[16]   Mortensen P, Andersson H, Gillissen J, Boersma B 2008 *Phys. Fluids* **20** 093302
[17]   Mortensen P, Andersson H, Gillissen J, Boersma B 2008 *Int. J. Multiph. Flow* **34** 678–683
[18]   Dearing S, Campolo M, Capone A, Soldati A 2013 *Exp. Fluids* **54** 1419
[19]   Cheng, Y, Pothos, S,Diez FJ 2010 *Exp. Fluids* **49** 1375-1391
[20]   Kasagi N, Matsunaga A 1995 *Int. J. Heat and Fluid Flow* **16** 477-485
[21]   Kulick JD, Fessler JR, Eaton JK 1994 *J. Fluid Mech.* **277** 109-134
[22]   Van Hout R 2011 *Int. J. Multiphase Flow* **37** 346–357
[23]   Stover CA, Cohen C 1990 *Rheol. Acta* **29** 192-203
[24]   Krochak P, Olson J, Martinez D 2010 *J. Fluid Mech.* **653** 431-462
[25]   Capone A, Romano GP, Soldati A 2014 *Exp. Fluids* **56** 1
[26]   Parsa S, Guasto J, Kishore K, Ouellette N, Gollub J, Voth G 2011 *Phys. Fluids* **23** 043302